

Six detached white-dwarf close binaries[★]

L. Morales-Rueda^{1,2}, T. R. Marsh^{3,2}, P. F. L. Maxted^{4,2}, G. Nelemans^{5,1}, C. Karl⁶
 R. Napiwotzki⁷, C. K. J. Moran²

¹*Department of Astrophysics, University of Nijmegen, P.O. Box 9010, 6500 GL Nijmegen, The Netherlands (lmr@astro.kun.nl)*

²*Department of Physics and Astronomy, University of Southampton, Southampton SO17 1BJ, UK*

³*Department of Physics, University of Warwick, Coventry, CV4 7AL, UK (T.R.Marsh@warwick.ac.uk)*

⁴*School of Chemistry and Physics, Keele University, Staffordshire ST5 5BG, UK (pflm@astro.keele.ac.uk)*

⁵*Institute of Astronomy, Madingley Rd, University of Cambridge, Cambridge CB3 0HA, UK*

⁶*Dr Remeis-Sternwarte, Astronomisches Institut der Universität Erlangen-Nürnberg, Sternwarstrasse 7, 96049 Bamberg, Germany*

⁷*Department of Physics & Astronomy, University of Leicester, University Road, Leicester LE1 7RH, UK*

Accepted 0000 000 00; Received 0000 000 00; in original form 0000 000 00

ABSTRACT

We determine the orbits of four double degenerate systems (DDs), composed of two white dwarfs, and of two white dwarf – M dwarf binaries. The four DDs, WD1022+050, WD1428+373, WD1824+040, and WD2032+188, show orbital periods of 1.157155(5) d, 1.15674(2) d, 6.26602(6) d and 5.0846(3) d respectively. These periods combined with estimates for the masses of the brighter component, based on their effective temperatures, allow us to constrain the masses of the unseen companions. We estimate that the upper limit for the contribution of the unseen companions to the total luminosity in the four DDs ranges between 10 and 20 per cent. In the case of the two white dwarf - M dwarf binaries, WD1042–690 and WD2009+622, we calculate the orbital parameters by fitting simultaneously the absorption line from the white dwarf and the emission core from the M-dwarf. Their orbital periods are 0.337083(1) d and 0.741226(2) d respectively. We find signatures of irradiation on the inner face of WD2009+622’s companion. We calculate the masses of both components from the gravitational redshift and the mass-radius relationship for white dwarfs and find masses of 0.75 – 0.78 M_{\odot} and 0.61 – 0.64 M_{\odot} for WD1042–690 and WD2009+622 respectively. This indicates that the stars probably reached the asymptotic giant branch in their evolution before entering a common envelope phase. These two white dwarf - M dwarf binaries will become cataclysmic variables, although not within a Hubble time, with orbital periods below the period gap.

Key words:

binaries: close – binaries: spectroscopic – white dwarfs

1 INTRODUCTION

About 10 per cent of white dwarfs reside in close binary systems (Napiwotzki et al. 2003). The formation of white-dwarf close-binary systems commences with a pair of main-

sequence stars orbiting in a wide binary. The most massive star will evolve faster becoming a giant and transferring mass to its companion. If mass transfer is sufficiently rapid, the result will be the formation of a common envelope (CE) made of the outer layers of the giant. The orbital energy of the binary can then be used to eject the envelope, the result being a binary composed of a white dwarf and a main sequence companion. If the mass ratio of the initial components was close to unity, the binary formed after CE ejection can still be wide, whereas in the case of extreme mass ratios, the two components will spiral in to eject the envelope forming a tighter binary. This binary, called a post common envelope binary (PCEB), if close enough, might become a cataclysmic variable (CV) if mass is transferred stably from

★ The Isaac Newton and William Herschel telescopes are operated on the island of La Palma by the Isaac Newton Group in the Spanish Observatorio del Roque de los Muchachos of the Instituto de Astrofísica de Canarias. Based on observations collected at the Centro Astronómico Hispano Alemán (CAHA) at Calar Alto, operated jointly by the Max-Planck Institut für Astronomie and the Instituto de Astrofísica de Andalucía (CSIC). Based on observations collected with ESO telescopes at the Paranal Observatory under programme IDs 165.H.-0588 and 167.D-0407.

the main sequence star to the white dwarf. If, on the other hand, the binary is too wide to become a CV, the main sequence star will evolve into a giant and the system will undergo another CE phase. When the envelope is ejected, the resulting binary will be composed of two white dwarfs a few solar radii apart - called a double degenerate (DD). For details on the evolution and formation of DDs see Nelemans et al.'s (2001) recent population synthesis studies and references therein. The study of white-dwarf close-binary stars can help us understand the elusive CE phase that they must have gone through, at least once, during their evolution. This phase is very difficult to study in any other manner as it lasts only of the order of 1 to 100 years. For recent calculations on CE ejection efficiencies see Soker & Harpaz (2003) and references therein.

The subjects of this paper, white dwarf - M dwarf binaries and DDs, are, as mentioned above, the progenitors of CVs, and potential progenitors of Type Ia supernova respectively. A short period DD where the combined mass of the white dwarfs exceeds the Chandrasekhar mass might become a Type Ia supernova (Iben & Tutukov 1984), but no candidates have yet been found. We should mention that this idea is still quite controversial with some theorists claiming that a DD does not become a Type Ia supernova (Saio & Nomoto 1998) and others claiming that this can be the case if one includes rotation in the calculations (Piersanti et al. 2003). The ESO Supernova Ia Progenitor Survey (SPY) has as its main goal to search systematically for massive, short period DDs in the galaxy to establish their direct link with Type Ia supernova and it is the source of more than 100 recently discovered DD systems (Napiwotzki et al. 2003). Efforts are also been carried out to systematically find white - M dwarf binaries by using the Sloan Digital Sky Survey (SDSS) resulting in more than 400 possible candidates (Silvestri, Hawley & Szkody 2003).

Schreiber & Gänsicke (2003) review the evolution of the known sample of white-dwarf close binaries with main sequence companions, the PCEBs, and conclude that, due to selection effects, the (until then) known population of PCEBs is dominated by young systems with hot white dwarfs that will evolve into short period CVs ($P < 3$ h). The PCEB sample is biased toward low mass companions as well which is the reason why they evolve into short period CVs. In contrast, the PCEBs found in the SDSS (Raymond et al. 2003), published later on, show an average white dwarf temperature significantly lower, demonstrating that to sample the full parameter space better selection criteria have to be devised.

In this paper we study 6 white dwarf close-binary stars. Four of them are found to be DDs, the other two are composed of a white dwarf and an M dwarf star. The separation of both components in these binaries is of the order of a few solar radii, as determined from their short orbital periods, so they are detached systems where no mass transfer between them takes place. We obtain their orbital solutions and compare the results obtained with predictions drawn from population synthesis studies.

Table 1. Journal of observations. A description of the setup used with each telescope is given in the text. N indicates the number of spectra taken with each setup. * indicates high resolution spectra covering only the emission core of $H\alpha$. The brightness in B magnitudes of each target is also given.

Object	N	Date	Setup	Inst.
WD1022+050 (B = 14.37)	10	29/2-3/3/96	AAT	RGO
	3	19/3/97	AAT	RGO
	6	8-10/2/98	INTa	IDS
	2	5/6/98	AAT	RGO
	2	15/4/03	INTb	IDS
WD1428+373 (B = 14.9)	2	16/2/97	INTb	IDS
	4	9-10/2/98	INTa	IDS
	9	3-5/3/99	INTa	IDS
	8	23/7/00	WHT	ISIS
	2	23/1/03	WHT	ISIS
WD1824+040 (B = 14.00)	13	19-24/6/95	INTa	IDS
	13	29/2-3/3/96	AAT	RGO
	17	18-21/3/97	AAT	RGO
	2	23-24/6/97	INTa	IDS
	2	17-18/5/00	VLT	UVES
	5	4/5-18/8/01	VLT	UVES
	10	26-30/10/01	INTa	IDS
WD2032+188 (B = 15.30)	5	23-27/2/02	3.5m	TWIN
	10	12-24/6/93	WHT	ISIS
	3	14-15/8/93	WHT	ISIS
	8	10-12/6/95	WHT	ISIS
	1	6/11/97	INTa	IDS
	1	22/11/97	WHT	ISIS
WD1042-690 (B = 13.05)	2	15/4/03	INTb	IDS
	15	29/2-3/3/96	AAT	RGO
WD2009+622 (B = 15.00)	5	18-20/3/97	AAT	RGO
	4*	10/6/96	WHT	UES
	6	21-25/6/95	INTa	IDS
	6	11/7/98	WHT	ISIS
	8	14/7/98	WHT	ISIS
7	6-7/10/98	WHT	ISIS	

2 OBSERVATIONS AND REDUCTION

The data used in this study were taken over many years (since 1993) using five different telescopes and seven different setups. Table 1 gives a list of the number of spectra taken for each target at each observing campaign indicating also which telescope was used in each case.

AAT: denotes data taken with the Royal Greenwich Observatory (RGO) spectrograph at the 4 m Anglo-Australian Telescope (AAT). The setup consisted of the 82 cm camera with the R1200R grating centred in $H\alpha$. The CCD used was an MIT-LL (3kx1k) in fast readout mode. This combination gives a dispersion of $0.23 \text{ \AA pixel}^{-1}$.

INTa: denotes data taken with the Intermediate Dispersion Spectrograph (IDS) at the 2.5m Isaac Newton Telescope (INT) on the island of La Palma. For these data, the setup consisted of the 500 mm camera with the R1200R grating centred in $H\alpha$ and the Tek (1kx1k) chip. This combination results in a dispersion of $0.39 \text{ \AA pixel}^{-1}$.

INTb: denotes data taken also with the IDS at the INT but with a setup that consisted of the 235 mm camera with the R1200B grating and the EEV10 (2kx4k) CCD. The

wavelength range covered in this case included $H\gamma$ and $H\beta$. This combination results in a dispersion of $0.48 \text{ \AA pixel}^{-1}$.

WHT: denotes spectra taken with the 4.2m William Herschel Telescope (WHT) on La Palma. Most of the spectra were obtained using the double arm spectrograph ISIS. Only the red spectra were used in our study. Except for the spectra taken in January 2003, the setup for the red arm consisted of the 500 mm camera with the R1200R grating and a Tek CCD (1kx1k) giving a dispersion of $0.40 \text{ \AA pixel}^{-1}$. For the spectra of WD1428+373 taken in January 2003, a MARCONI CCD (2kx4.7k) was used giving a dispersion of $0.23 \text{ \AA pixel}^{-1}$. In the case of the 4 high resolution spectra taken of WD2009+622 (marked with a star in Table 1), the Utrecht Echelle spectrograph (UES) was used with the 35 cross disperser and a Tek (1kx1k) CCD giving a typical dispersion of $0.07 \text{ \AA pixel}^{-1}$.

VLT: denotes data taken with the UV-Visual Echelle Spectrograph (UVES) at the UT2 (Kueyen) VLT 8.2 m telescope located at Paranal Observatory. The setup used consisted of Dichroic 1 (central wavelengths 3900 \AA and 5640 \AA) with a EEV CCD (2kx4k) for the blue arm and two CCDs, a EEV (2kx4k) and a MIT-LL (2kx4k) for the red arm. This setup allows us to achieve almost complete spectral coverage from 3200 \AA to 6650 \AA with only two $\sim 80 \text{ \AA}$ wide gaps at 4580 \AA and 5640 \AA . A slit width of 2.1" was used to minimise slit losses and the CCDs were binned 2×2 to reduce readout noise. This setup results in a spectral resolution of 0.36 \AA (or better if the seeing disk is smaller than the slit width) at $H\alpha$. Exposure times were 5 min.

3.5 m: denotes data taken with the double beam TWIN spectrograph at the 3.5 m telescope in the Calar Alto Observatory. Only the red spectra were used in this paper. The setup for the red arm consisted of the 230 mm camera with the T06 grating (1200 grooves mm^{-1}) and a SITE-CCD (2kx0.8k) giving a dispersion of $0.55 \text{ \AA pixel}^{-1}$.

The slit width was set to values between 0.8 and 1 arcsec depending on the seeing. We made sure in every case that the star filled the slit to avoid systematic errors in the radial velocities caused by the star wandering in the slit during an exposure.

For the AAT, INT, and WHT runs we obtained CuAr plus CuNe frames to calibrate the spectra in wavelength. In the case of the 3.5 m and VLT observations the wavelength calibration arc used was a ThAr. All target spectra were bracketed by arc spectra taken within one hour and the wavelength scale interpolated to the time of mid-exposure. We subtracted from each image a constant bias level determined from the mean value in its over-scan region. Tungsten flatfield frames were obtained each night to correct for the pixel to pixel response variations of the chip. Sky flatfields were also obtained to correct for the pixel to pixel variations of the chip along the slit. After debiasing and flatfielding the frames, spectral extraction proceeded according to the optimal algorithm of Marsh (1989). The arcs were extracted using the profile associated with their corresponding target to avoid systematic errors caused by the spectra being tilted. Uncertainties on every point were propagated through every stage of the data reduction. We did not attempt to correct for light losses in the slit. For the VLT spectra a special procedure was applied to correct for a quasi-periodic ripple pattern appearing in many of the uncorrected merged spectra (Napiwotzki et al. 2005). The resulting VLT spectra

were then divided by a smoothed spectrum of a DC white dwarf, which by definition shows no spectral features at all and therefore provides an excellent means of correcting for the instrumental response.

3 RESULTS

3.1 Average spectra

Fig. 1 presents the average red spectra for the six systems discussed in this paper. The spectra of four of the systems, WD1022+050, WD1428+373, WD1824+040 and WD2032+188, are very similar showing only very broad absorption at $H\alpha$. WD1042–690 and WD2009+622, on the other hand, show a double line structure in their $H\alpha$ line profile composed of broad absorption coming from the white dwarf and narrow emission from the heated surface of the M dwarf companion. As this narrow emission moves within the absorption profile with the orbital period, an average spectrum would show the emission broadened and for that reason for these two systems we present the spectrum at a particular orbital phase instead of an average of the spectra during an orbit. The narrow emission in WD1042–690 is, on average, significantly stronger than for WD2009+622. For WD2009+622, the strength of the narrow emission core changes with orbital phase and only at orbital phase 0.5 (when we are looking directly into the heated face of the M dwarf) reaches similar strength to that in WD1042–690. See Section 3.3.1 for details.

3.2 Four double degenerate systems

To measure the radial velocities of the four double degenerates: WD1022+050, WD1428+373, WD1824+040 and WD2032+188, we used least squares fitting of a model line profile. The model line profile is the summation of three Gaussian profiles with different widths and depths. For any given star, the widths and depths of the Gaussians are optimised and then held fixed while their velocity offsets from the rest wavelengths of the lines in question are fitted separately for each spectrum; see Maxted, Marsh & Moran (2000c) for further details of this procedure.

Once the radial velocities for each system were known (see Table 2) we used a “floating mean” periodogram to determine the periods of our targets (e.g. Cumming, Marcy & Butler 1999). The method consists in fitting the data with a model composed of a sinusoid plus a constant of the form:

$$\gamma + K \sin(2\pi f(t - t_0)),$$

where f is the frequency and t is the observation time. The key point is that the systemic velocity is fitted at the same time as K and t_0 . This corrects a failing of the well-known Lomb-Scargle (Lomb 1976; Scargle 1982) periodogram which starts by subtracting the mean of the data and then fits a plain sinusoid; this is not the best approach for small numbers of points. We obtained the χ^2 of the fit as a function of f and then identified minima in this function.

Table 3 gives a list of the orbital parameters derived for each DD binary star. The orbital period of the second best alias is also given, along with the difference in χ^2 between

Table 2. Radial velocities for the 5 systems. In the case of the 2 white dwarf-M dwarf systems the values given are measured from the M dwarf.

HJD - 2440000	RV (km s ⁻¹)	HJD - 2440000	RV (km s ⁻¹)	HJD - 2440000	RV (km s ⁻¹)
WD1022+050		WD1824+040		WD2032+188	
10143.1257	-32.23±2.55	9893.4920	96.12± 3.76	9162.5641	42.79±5.58
10143.1447	-34.08±3.03	9893.4999	95.64± 4.97	9162.5752	52.97±5.51
10144.0893	20.85±2.67	10143.2756	58.98± 2.83	9162.6371	54.49±4.82
10144.1012	16.48±2.46	10143.2818	56.00± 3.20	9162.6485	53.30±5.03
10145.0577	89.35±1.96	10143.2880	52.64± 2.81	9214.5046	97.72±4.18
10145.0697	81.96±2.01	10143.2949	51.37± 3.05	9214.5220	99.70±4.15
10146.0863	111.94±2.21	10144.2766	100.47± 1.85	9214.5414	102.52±4.47
10146.0983	116.99±2.04	10144.2851	100.91±1.96	9878.6788	-7.75±4.36
10146.1719	99.17±1.99	10144.2936	102.73±2.10	9878.6848	-5.62±4.46
10146.1839	97.42±2.22	10145.2760	101.46±2.65	9879.7064	62.70±8.39
10527.1487	5.75±3.16	10145.2892	99.27±3.30	9879.7136	61.99±7.84
10527.1584	8.34±3.63	10146.2791	58.95±2.54	9879.7207	72.30±8.73
10527.1670	5.32±3.83	10146.2862	57.30±2.88	9880.7100	98.97±7.60
10852.5812	-31.10±4.68	10146.2934	57.87±3.59	9880.7171	95.36±7.19
10852.5911	-41.51±3.72	10146.2986	54.33±8.30	9880.7270	98.67±7.50
10854.4604	56.58±4.83	10526.2345	89.86±1.74	10759.3259	57.43±8.35
10854.4688	66.99±4.17	10526.2465	92.02±1.68	10775.3924	97.21±3.23
10855.4728	109.75±3.07	10526.2585	96.23 ±1.81	12745.6895	-39.02±7.58
10855.4853	109.26±2.80	10526.2715	95.24±1.64	12745.7036	-22.83±6.93
10969.8494	102.51±3.08	10526.2835	94.06±1.60	WD1042-690	
10969.8567	107.65±3.09	10526.2955	92.74±1.36	10143.1591	76.49±0.39
12744.4589	-30.08±4.44	10526.3078	97.26±2.34	10143.1687	76.13±0.36
12744.4731	-40.03±4.63	10527.2658	109.40±4.04	10143.9950	-56.70±0.44
12746.5091	26.01±3.96	10527.2777	113.65±3.27	10144.0000	-57.84±0.44
12746.5232	23.86±4.21	10527.2898	109.12±2.87	10144.1363	57.57±0.54
WD1428+373		10527.2995	109.09±4.06	10144.1401	61.33±0.56
10495.7128	-40.29±7.71	10528.2664	63.33±3.97	10144.2244	54.00±0.48
10495.7230	-29.57± 8.36	10528.2809	69.52±3.61	10144.2586	9.87±0.54
10853.7482	-7.31± 3.91	10529.2823	10.56±42.73	10144.2625	5.78±0.57
10853.7658	-10.22± 3.99	10529.2931	9.85±2.60	10144.2663	-1.43±0.67
10854.6999	40.78± 3.68	10529.3025	5.22±3.03	10144.2702	-3.85±0.57
10854.7709	34.01± 3.39	10529.3095	12.36±5.84	10145.0378	-58.52±0.55
11240.5750	-79.23± 6.07	10622.5164	50.08±3.68	10145.0416	-56.30±0.47
11240.6267	-65.38± 3.68	10623.7062	-6.21±4.38	10145.9757	-29.74±0.58
11240.7237	-11.07± 3.80	11681.7165	35.50±1.12	10145.9808	-34.51±0.57
11241.5861	-81.31± 3.88	11682.8933	-15.40±0.79	10526.1651	20.20±0.47
11241.6592	-89.18± 3.36	12033.8514	-13.50±1.12	10527.1754	21.97±0.45
11241.7579	-54.58± 4.47	12078.7265	6.4±0.63	10528.1260	77.15±0.75
11242.5826	-57.44± 3.76	12116.5747	21.30±0.52	10528.1406	69.36±0.92
11242.7032	-88.63± 3.89	12117.5939	81.90±0.56	10528.1558	59.51±1.04
11242.7749	-92.46± 4.03	12139.5163	13.20±2.44	WD2009+622	
11749.3945	-95.69± 1.98	12209.3141	-12.86±1.41	9889.6260	-25.63±3.04
11749.4086	-88.57± 2.23	12209.3241	-15.21±1.51	9891.6758	50.04±3.81
11749.4247	-95.29± 2.09	12210.3159	7.46±1.67	9892.6414	-93.00±3.41
11749.4388	-91.40± 2.05	12210.3322	14.18±1.04	9892.6633	-123.83±3.55
11749.4580	-84.93± 2.05	12210.3579	12.56±1.59	9893.6384	-208.76±4.27
11749.4721	-79.71± 2.10	12211.3070	60.44±1.68	9893.6603	-188.42±3.83
11749.4885	-73.10± 2.28	12211.3198	65.92±1.34	10244.6034	32.39±1.61
11749.5026	-70.89± 2.25	12211.3344	69.37±1.27	10244.6270	12.99±1.63
12663.7233	40.86±4.25	12212.3669	110.82±1.33	10244.6798	-38.75±1.68
12663.7801	42.97±4.43	12213.3830	80.96±2.12	10244.7081	-77.49±1.73
WD1824+040		12328.7068	-18.31±1.22	11005.7017	27.46±2.33
9887.5980	91.57± 12.09	12329.6908	22.18±2.56	11005.7077	35.25±2.31
9887.6209	99.20± 14.57	12330.7425	86.05±1.75	11005.7136	38.70±2.18
9887.6529	106.03± 4.25	12331.7437	102.40±3.32	11005.7213	33.43±2.22
9888.5371	95.16± 2.44	12332.7505	85.59±3.65	11005.7272	44.31±2.30
9888.5455	94.28± 3.47	WD2032+188		11005.7324	33.92±3.87
9889.5252	45.32± 2.24	9150.6424	-40.70±6.83	11008.6761	34.63±2.64
9889.5332	41.20± 3.19	9150.6533	-18.85±6.08	11008.6820	41.52±2.57
9891.5276	-2.10± 2.48	9150.6677	-21.41±6.37	11008.6879	41.85±2.57
9891.5356	-0.29± 3.63	9150.6788	-20.83±7.99	11008.6939	40.15±2.60
9892.5007	41.05± 4.06	9153.6509	95.30±11.16	11008.7012	44.00±2.78
9892.5087	37.97± 3.87	9153.6702	100.11±9.50	11008.7072	51.42±2.76

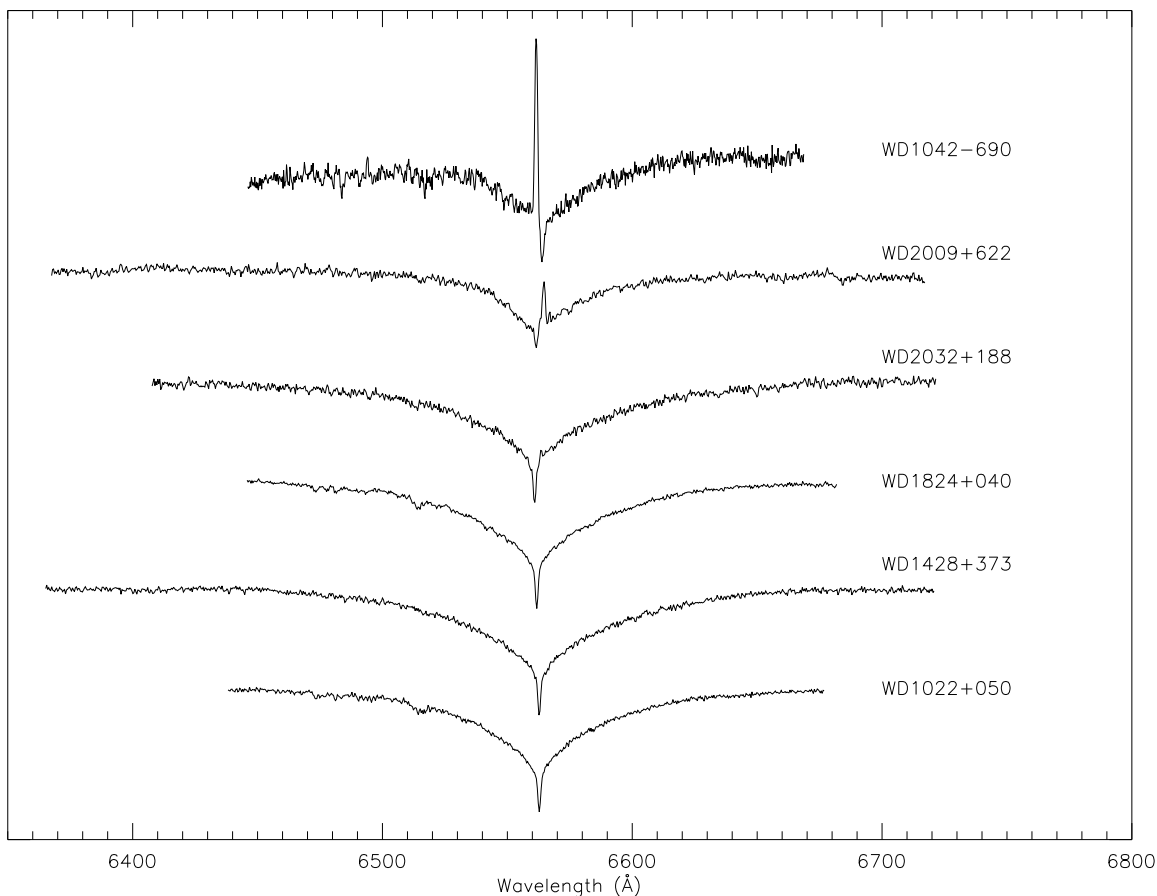


Figure 1. Average spectra for the six systems studied in this paper.

Table 2. Continued.

HJD - 2440000	RV (km s ⁻¹)	HJD - 2440000	RV (km s ⁻¹)	HJD - 2440000	RV (km s ⁻¹)
WD2009+622					
11008.7131	42.67±2.73				
11008.7190	50.81±2.59				
11093.4111	-76.67±3.14				
11093.4748	-146.25±5.21				
11093.5206	-194.63±3.10				
11093.5673	-224.30±3.29				
11094.3644	-232.52±2.78				
11094.4819	-164.87±2.82				
11094.5644	-50.85±3.58				

Table 3. List of the orbital periods measured for the four double degenerate systems studied. T_0 , the systemic velocity, γ , the radial velocity semi-amplitude, K , the reduced χ^2 achieved for the best alias, the 2nd best alias and the χ^2 difference between the 1st and 2nd aliases are also presented. When calculating the χ^2 for both aliases we have added in quadrature a systematic error that results in a reduced $\chi^2 \sim 1$ (see text for details). The number of data points used to calculate the orbital period is given in the final column under N .

Object	HJD (T_0) -2400000	Period (d)	γ (km/s)	K (km/s)	$\chi^2_{reduced}$	2nd best alias (d)	$\Delta\chi^2$	N
WD1022+050	51445.262(5)	1.157155(5)	39.05±1.19	74.77±1.16	1.25	8.1580(4)	40	25
WD1428+373	51579.64(1)	1.15674(2)	-21.46±1.62	67.90±1.68	1.41	1.22640(1)	42	25
WD1824+040	51108.192(9)	6.26600(5)	47.95±0.40	61.87±0.55	1.24	0.5449639(5)	3064	67
WD2032+188	50947.07(5)	5.0846(3)	35.11±1.52	63.50±1.59	0.66	9.8267(6)	45	25

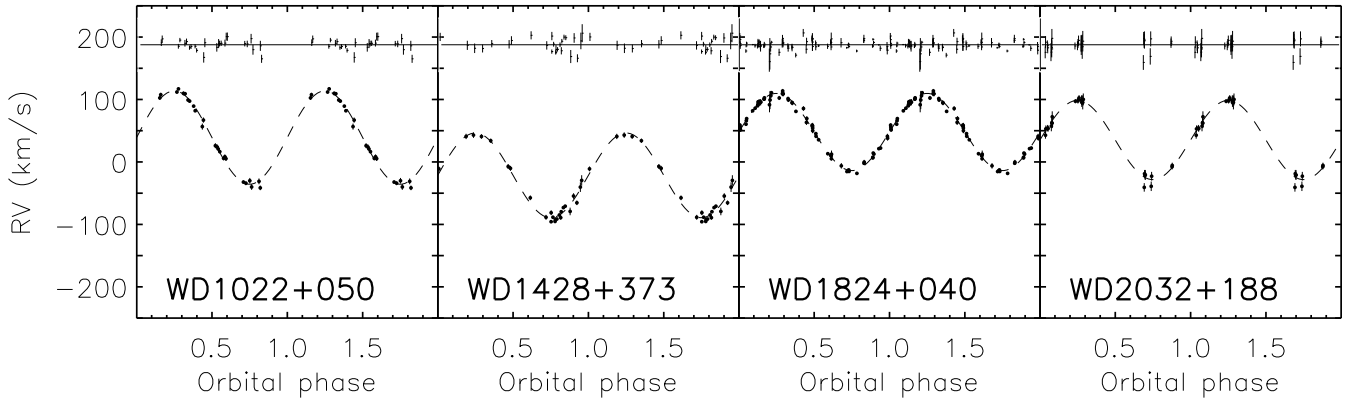


Figure 2. Radial velocity curves for the four double degenerate systems. The data have been folded on the orbital period in each case. See Table 3 for the list of periods, radial velocity semiamplitudes and systemic velocities. Included in each panel is a plot of the residuals to the fit. The vertical scale on which the residuals have been plotted is twice the scale on which the radial velocities are plotted.

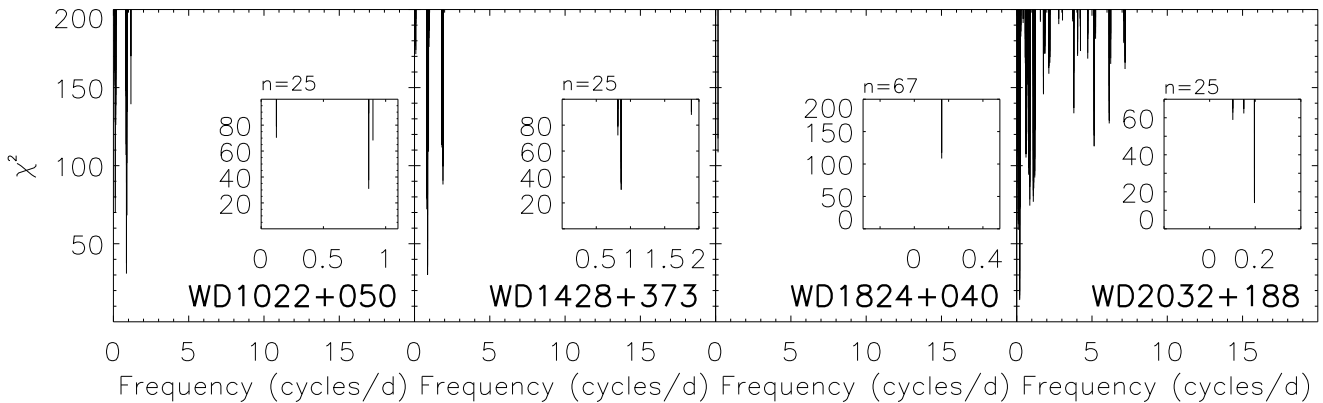


Figure 3. Each panel presents χ^2 versus cycles/day obtained after the period search was carried out. The frequency with the smallest χ^2 corresponds to the orbital frequency of the system. For clarity we have also included an inset showing a blow up of the region where the best period is. The number of radial velocity measurements used for the period search calculations, n , is shown in each panel.

the two best periods found. The large difference in χ^2 indicates that the second best aliases are not plausible. The resulting radial velocity curves (folded in the orbital period) are presented in Fig. 2 and the corresponding periodograms (χ^2 versus orbital frequency) in Fig. 3. Each panel in the periodogram includes a blow up of the region in frequency where the minimum χ^2 is found.

In each case, we compute the level of systematic uncertainty that when added in quadrature to our raw error estimates gives a reduced $\chi^2 \sim 1$. By doing this we are considering the un-accounted sources of error such as true variability of the star or slit-filling errors that cause the poor fits of a few stars. Such errors are unlikely to be correlated with either the orbit or with the statistical errors we estimate, and therefore we add a fixed quantity in quadrature with our statistical errors as opposed to applying a simple multiplicative scaling to them. In all cases we use a minimum value of 2 km s^{-1} corresponding to $1/10^{\text{th}}$ of a pixel

which we believe to be a fair estimate of the true limits of our data. The last column of Table 4 gives the value of systematic uncertainty that we have added in quadrature in each case.

We then calculate the probability of the true orbital periods being further than 1 and 10 per cent from the values we obtained - see Morales-Rueda et al. (2003a) and Marsh, Dhillon & Duck (1995) for an explanation of the method used to calculate these probabilities - and present them in Table 4.

In all cases, the probabilities of the quoted periods being wrong are very low and we are certain that the values given in Table 3 correspond to the true orbital solution.

In the cases where the probability of the orbital period being further than 1 and 10 per cent from our favoured value is the same, the significant probability lies within a very small range around the best period, with all the significant

Table 4. List of probabilities that the true orbital period of a system lies further than 1 and 10 per cent from our favoured value given in Table 3. Numbers quoted are the logarithms in base 10 of the probabilities. Column number 4 gives the value of the systematic uncertainty that has been added in quadrature to the raw error to give a reduced $\chi^2 \sim 1$.

Object	1%	10%	systematic error (km s ⁻¹)
WD1022+050	-7.66	-7.69	3
WD1428+373	-9.59	-13.08	4
WD1824+040	-1000	-1000	2
WD2032+188	-9.89	-9.90	2

Table 5. The mass functions, f_m , of the unseen components together with the larger lower limits obtained by assuming $i = 90^\circ$ and by substituting in the mass function equation our determination of the mass of the brighter component, M_1 .

Object	$f_m(M_\odot)$	$M_1(M_\odot)$	$M_2(M_\odot)$ lower limit
WD1022+050	0.050	0.389	0.283
WD1428+373	0.038	0.348	0.233
WD1824+040	0.154	0.428	0.515
WD2032+188	0.135	0.406	0.469

competition (i.e. next best alias) placed outside the 10 per cent region around the best alias.

3.2.1 The unseen component of the binary

By knowing the radial velocity semiamplitude of one of the components of the binary (the observable component), K , and the orbital period of the system, we can then calculate the mass function of the unseen component by using:

$$f_m = \frac{M_2^3 \sin^3 i}{(M_1 + M_2)^2} = \frac{PK_1^3}{2\pi G}, \quad (1)$$

where the subscripts “1” and “2” refer to the brighter and the dimmer components respectively. The mass function is the lower limit of the mass of the unseen component. Table 5 gives the mass functions of the unseen components for the four DDs studied. In two cases (WD1824+040 and WD2032+188) the companion’s mass function is greater than $0.1M_\odot$ which corresponds to the mass of a late M dwarf if it is a main sequence star. The masses of the brighter components of the systems have been measured by fitting their hydrogen line profiles to stellar atmosphere models using the tracks by Althaus & Benvenuto (1997) and can be substituted, together with the assumption of the orbital inclination of the system being 90° , in the mass function equation to give a larger lower limit for the masses of the unseen components. These revised lower limits (also presented in Table 5) are all greater than $0.1M_\odot$ which indicates that the unseen companions cannot be main sequence stars because if they were we should be able to detect them (Marsh et al. 1995). The unseen companions must therefore be also compact objects, probably white dwarfs.

We searched for the signature of the faint companions by shifting out the fitted radial velocity for each binary

and then looking for differences in the line profiles at the quadrature phases (Marsh et al. 1995), i.e. 0.25 and 0.75. The spectra at quadrature phases were obtained by averaging the spectra contained in two separate phase ranges, i.e. the spectra in the range from 0.1 to 0.4 were averaged to obtain the phase 0.25 spectrum, and the spectra in the range from 0.6 to 0.9 to obtain the phase 0.75 spectrum. The results are plotted in Fig. 4. Any contribution from the companion white dwarf should be seen as an asymmetry in the line profile at phase 0.25 that is mirrored at phase 0.75 with respect to the rest wavelength (Marsh et al. 1995). None of the four systems show a clear asymmetry of this type in the line profiles.

A second test that can be carried out to look for the faint companion consists in shifting out the fitted radial velocity off the spectra and creating a mean spectrum by combining all the shifted spectra, subtracting this mean spectrum from the individual shifted ones and plotting the resulting spectra in a stack or trail. This aids the eye to identify any leftover absorption moving with the binary orbit. A Doppler map (Marsh & Horne 1988) can also be computed from these stack of spectra. Any orbital motion leftover in the spectra would appear in the maps as a small absorption region located in the $V_x = 0$ axis of the velocity map. We do not find any indication of the presence of the unseen component in either trails or Doppler maps in any of the four systems studied.

3.2.2 How faint is the unseen companion?

We explore the question of how small the contribution of the faint component of the system has to be so as not to be detected using the methods discussed in the previous section.

To answer this question we create synthetic spectra that include the absorption corresponding to the brighter component of the system (in the form of three Gaussians), scaled to the measured value for each system, plus some extra absorption moving opposite to it (also represented by three Gaussians) and determine for what percentage of brightness, relative to the bright component, we should be able to detect the faint component by looking at the spectra around the quadrature phases (Marsh et al. 1995). This method assumes that the companion stars have a spectrum similar to that of the brighter component. Although the fainter white dwarf is cooler and its H α line will be less deep in its spectrum, this seems like a reasonable assumption as the companions are also white dwarfs, unless of course they are not DA white dwarfs.

In the case of WD1022+050 we find that the brightness of the companion must be less than 10 per cent the brightness of the bright component for us not to detect it. The values we find for WD1428+373, WD1824+040, and WD2032+188 are 9 per cent, 23 per cent and 17 per cent respectively. These values translate into magnitudes for the companions, in the 6400–6700Å region, that are respectively 2.5, 2.6, 1.6 and 1.9 fainter than that of the bright components. Using the calculated absolute V magnitudes for the bright components (10.68, 10.35, 10.83 and 10.24, see the Discussion Section) and the broadband colour indices for pure hydrogen and $\log g = 8$ stellar atmosphere models computed by Bergeron, Wesemael & Beauchamp (1995), we

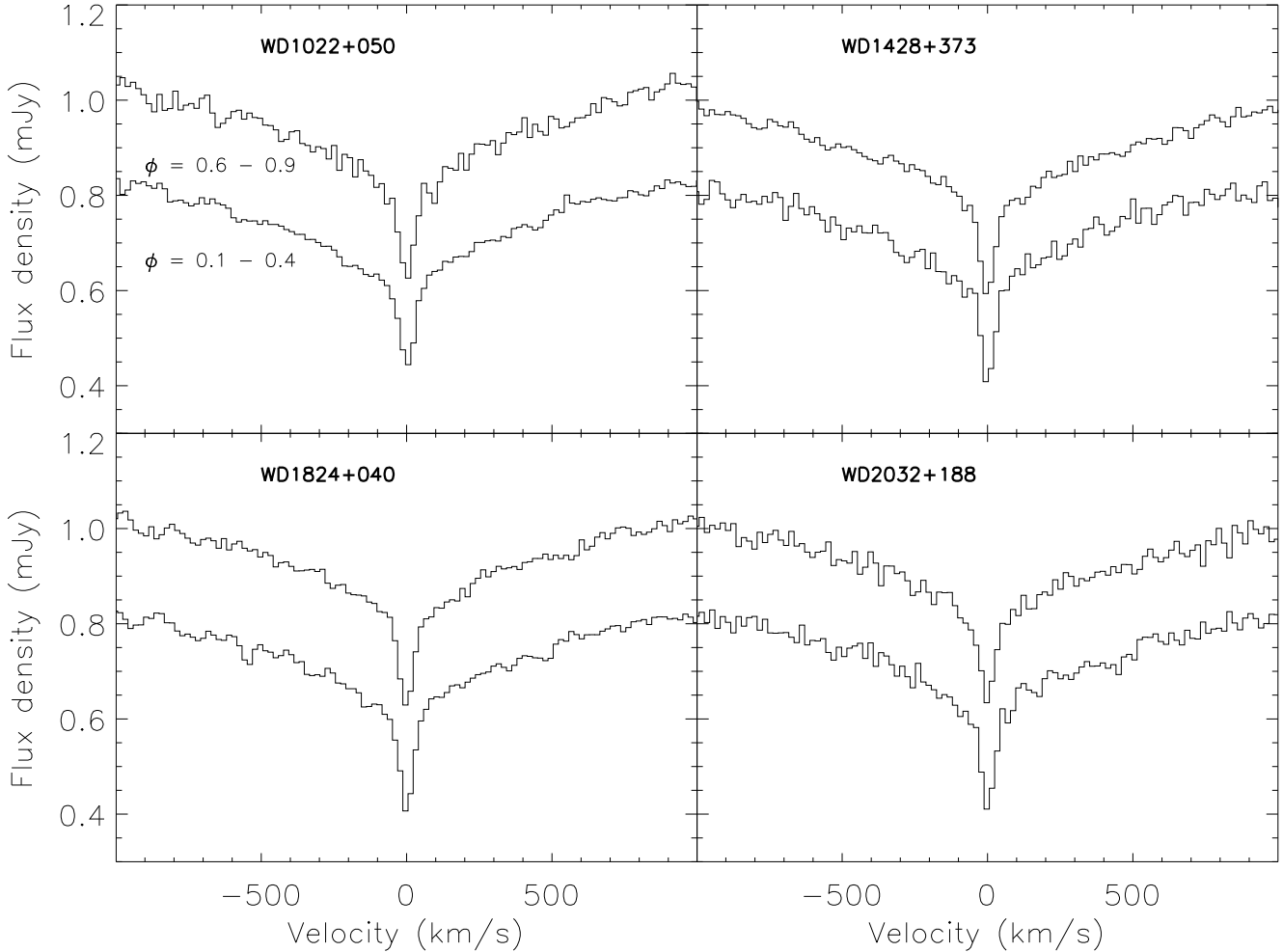


Figure 4. The spectra averaged around the quadrature phases for the four systems studied. In each case, the lower spectrum corresponds to quadrature phase 0.25 and the top one to phase 0.75. There is no clear asymmetry in the line profile at phase 0.25 that gets mirrored in phase 0.75 for any of the systems. This indicates that we cannot detect the faint companion of the systems.

obtain upper limits for the absolute R magnitudes of the faint components of 13.3, 13.0, 12.5 and 12.2 respectively.

3.3 Two white dwarf/M dwarf binaries

In the case of WD1042–690 (aka BPM 6502) and WD2009+622 the spectra are composed of absorption lines that have their origin in the white dwarf plus emission cores that have their origin in the M dwarf. This extra emission component makes the measuring of the radial velocities more complicated, as the absorption coming from the white dwarf has its core filled by the M dwarf emission. A way to measure simultaneously the radial velocities of both components is to use least squares fitting of a model line profile as in the previous case but this time using a model line profile that is the sum of four Gaussian profiles. Three of the Gaussians fit the absorption component and one fits the emission. The steps followed to carry out these complex fits consisted of: 1) fitting only the emission lines with a single Gaussian function and obtaining the radial velocities associated to the emission line for each spectrum, 2) calculating the orbital solution for the emission lines by means of obtaining a peridiogram from the radial velocities measured, 3) using this

orbital solution to fix the orbit of the three Gaussians that will fit the absorption component of the lines and 4) obtaining the radial velocity semi-amplitude and systemic velocity for the white dwarf by fitting all the spectra simultaneously with one emission and three absorption Gaussians.

This method was easily applicable to WD2009+622 as the emission coming from the M dwarf is comparable to the H α absorption core (see Fig. 1). In the case of WD1042–690 the emission component is very strong compared with the absorption core making the fitting of the data more difficult and the results obtained less accurate. For WD1042–690 we find 7 very close aliases with very similar values of χ^2 . Table 6 gives a list of the orbital solutions for the 7 aliases. The solutions for K_2 , γ_2 , K_1 and γ_1 are consistent within the errors for all aliases. Previous studies of WD1042–690 (Kawka et al. 2000) result in an orbit solution in which the orbital period is consistent with our alias number 3 and the values for K_2 , γ_2 , K_1 and γ_1 are consistent with those from our 7 aliases. In Table 7 we present the orbital solutions for WD1042–690 and WD2009+622. The results presented for WD1042–690 correspond to the first alias shown in Table 6. In Fig. 5 we plot the radial velocities measured for the emission and absorption components together with the best fits

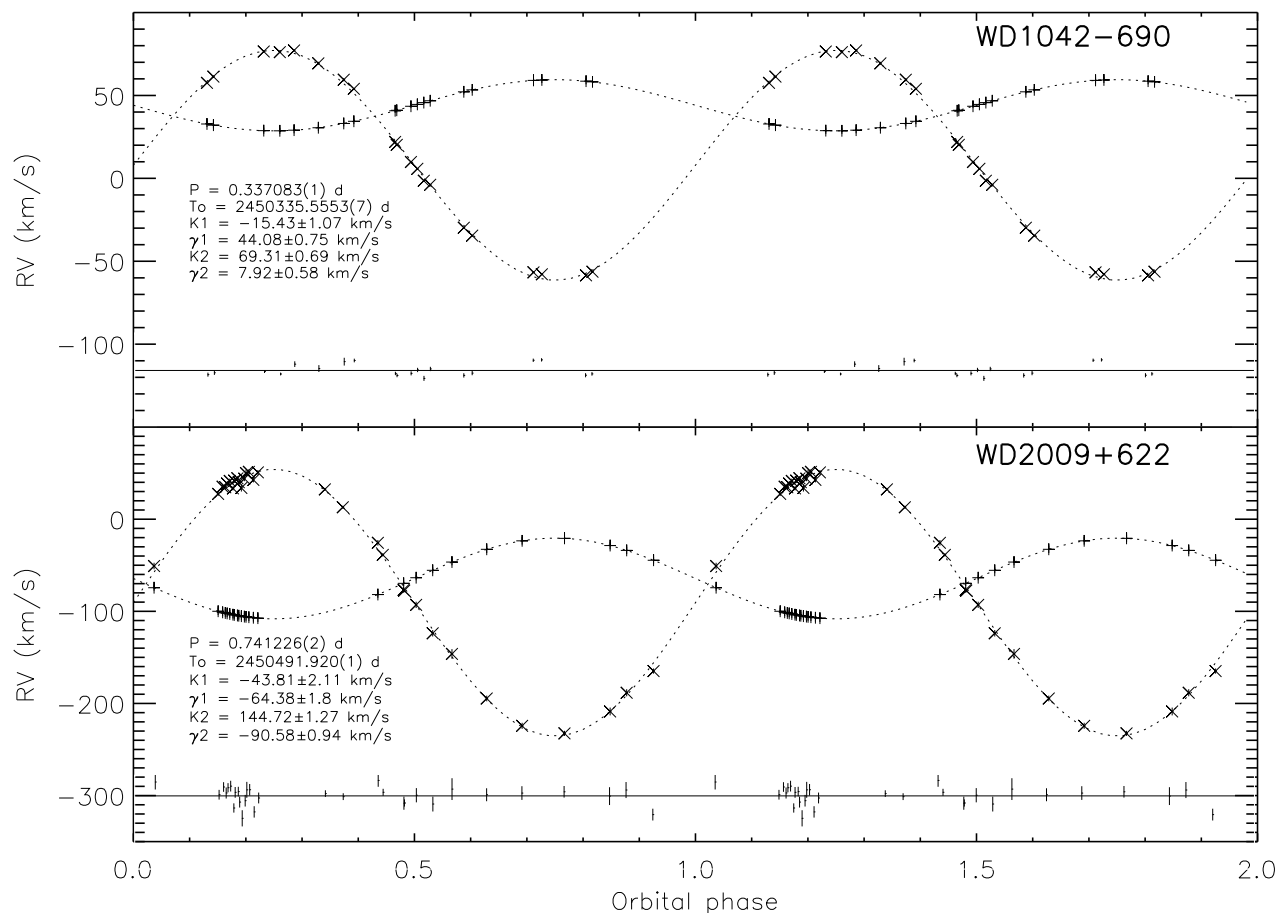


Figure 5. Orbital solution for WD1042–690 and WD2009+622. Included in each panel is a plot of the residuals to the fit to the emission line component. The vertical scale on which the residuals have been plotted is larger than the scale on which the radial velocities are plotted.

Table 6. Orbital solution for the 7 aliases found for WD1042–690.

P (d)	T_0 –2450000	γ_2	K_2	χ_{2red}^2
0.337083(1)	335.5553(7)	7.93 ± 0.58	69.31 ± 0.69	0.65
0.337380(1)	335.7239(7)	7.83 ± 0.58	69.24 ± 0.69	0.74
0.336786(1)	335.7239(7)	8.03 ± 0.58	69.38 ± 0.69	0.75
0.337678(1)	335.5550(7)	7.73 ± 0.58	69.16 ± 0.69	1.01
0.336490(1)	335.5557(7)	8.14 ± 0.58	69.44 ± 0.70	1.03
0.337977(1)	335.7238(7)	7.64 ± 0.58	69.07 ± 0.68	1.47
0.336194(1)	335.7240(7)	8.26 ± 0.58	69.49 ± 0.70	1.48

given in Table 7. The error bars in the radial velocities are smaller than the size of the symbols used to plot the data. Notice that there are 4 extra points in the fit to the radial velocity of the M dwarf for WD2009+622. This accounts for the 4 high resolution spectra taken with UES that only covered the core of the $H\alpha$ line.

Table 7. List of the orbital periods measured for the two white dwarf-M dwarf systems studied. T_0 , the systemic velocity, γ , the radial velocity semi-amplitude, K , for both the white dwarf and the M dwarf, and the reduced χ^2 achieved for the best alias are given. The number of data points used to calculate the orbital period is also given.

	WD1042–690	WD2009+622
N	20	31/27
P (d)	0.337083(1)	0.741226(2)
T_0 (d)	2450335.5553(7)	2450491.920(1)
K_{WD} (km s^{-1})	-15.43 ± 1.07	-43.81 ± 2.11
γ_{WD} (km s^{-1})	44.08 ± 0.75	-64.38 ± 1.80
K_M (km s^{-1})	69.31 ± 0.69	144.72 ± 1.27
γ_M (km s^{-1})	7.92 ± 0.58	-90.58 ± 0.94
χ_{2red}^2	0.65	1.12
$q = M_M/M_{WD}$	0.223 ± 0.018	0.303 ± 0.017

3.3.1 The M dwarf companions

We binned the spectra for both binary systems into 10 phase bins and plotted them in Fig. 6 as a stack of spectra with orbital phase in the vertical axis. The advantage of presenting the spectra in this way is that we can explore the line flux variations during an orbit. In the case of WD1042–690

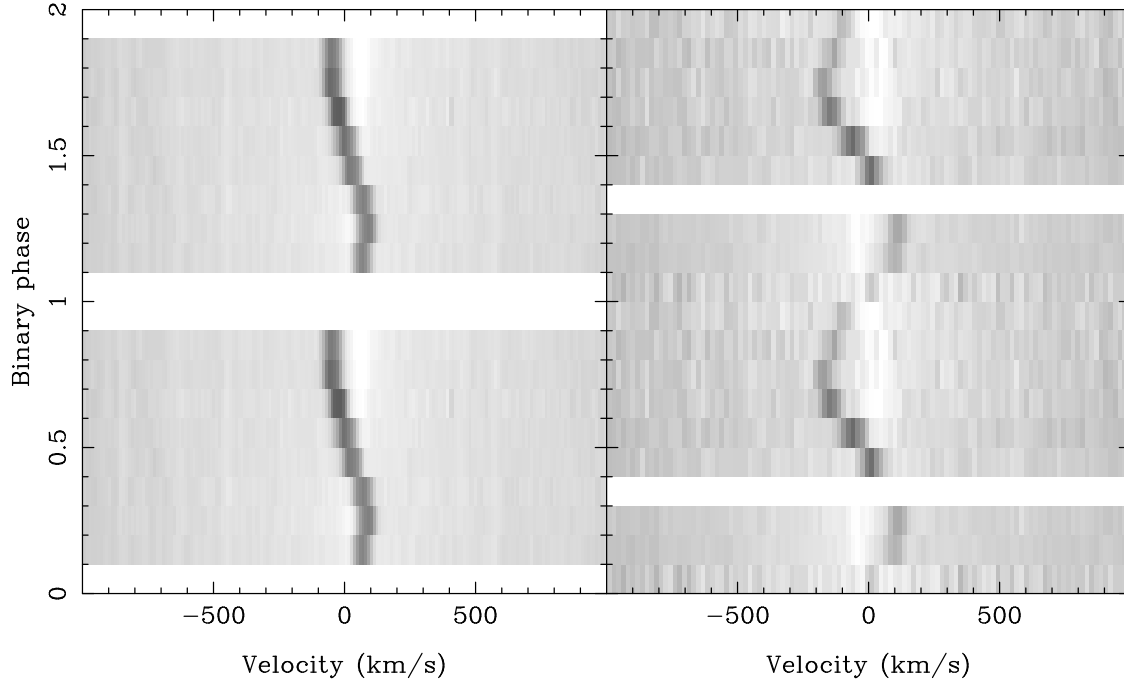
WD1042+690 H α WD2009+622 H α 

Figure 6. Trailed phase binned spectra for WD1042+690 and WD2009+622. The orbit is plotted twice. The variable brightness in the emission line component, coming from the M dwarf companion, is clear in WD2009+622.

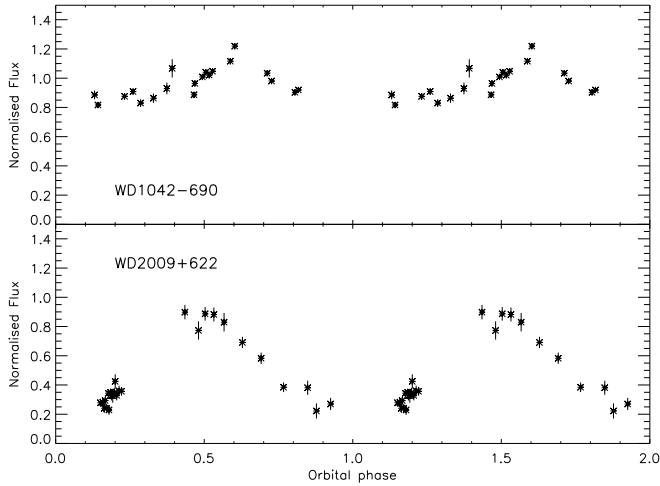


Figure 7. Flux modulation seen on the emission from the M dwarf component of WD1042+690 (top) and WD2009+622 (bottom).

the strength of the emission line does not vary significantly with orbital phase. This is not the case for WD2009+622 where the line flux increases at orbital phases around 0.5. This phase corresponds to the white dwarf and the M dwarf being aligned with the line of sight, the white dwarf being closer to us. At this phase we are looking to the heated face of the M dwarf.

To determine how the line flux varies with phase, we fitted the line profiles once more with four Gaussians, three

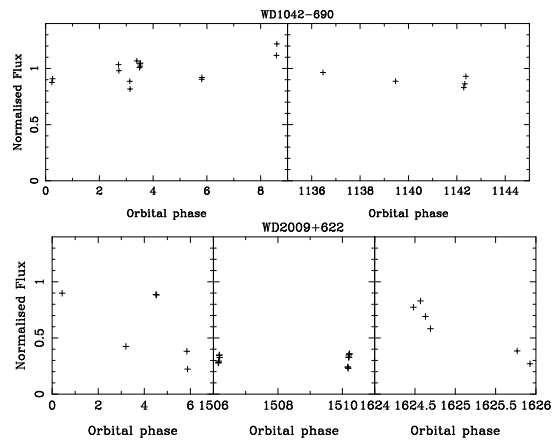


Figure 8. Flux modulation seen on the emission from the M dwarf component of WD1042+690 (top) and WD2009+622 (bottom). This time the data has not been folded in the orbital period.

for the absorption component and one for the emission component but this time we allowed the height of the emission component to vary. The results are displayed in Fig. 7. The variation in flux is very significant in WD2009+622 and as we mentioned earlier it can be explained with emission coming from the irradiated face of the M dwarf, the side facing the white dwarf. This has important consequences for the calculation of the mass of the white dwarf carried out in the following sections as we have to account for distortions on the M dwarf to correct its radial velocity semi-amplitude. When the companion is heavily irradiated the emission line

used to measure its radial velocity will give us the value associated with the irradiated face, not the value for the centre of mass of the companion. Maxted et al. (1998) find that probably as a result of optical depth effects, Balmer emission lines induced by irradiation are significantly broadened rendering measurements of radial velocities from fitting these lines more inaccurate.

In the case of WD1042–690, there is also some flux modulation present at a fainter level but peaking at phase 0.6 rather than phase 0.5. This is probably associated to chromospheric activity of the M dwarf rather than irradiation. To make sure that this variability is not orbital we have also plotted the flux of the emission component versus unfolded orbital phase in Fig. 8. We see that for WD1042–690 the variability observed is not phase dependent implying that is intrinsic to the M dwarf, probably chromospheric. In the case of WD2009+622 the variability observed is larger and it peaks at phase 0.5 confirming that it is due to irradiation of the inner face of the M dwarf by the white dwarf.

3.3.2 The masses of the components

Once the radial velocity semiamplitudes for both components have been measured, together with the orbital period we can use Eq. 1 to obtain the mass function for the white dwarf and the M dwarf in each case. If we combine Eq. 1 with $q = M_M/M_{WD} = K_{WD}/K_M$ we obtain larger lower limits for the masses of both components:

$$\begin{aligned} M_{WD} &= \frac{PK_M(K_{WD} + K_M)^2}{2\pi G \sin^3 i}, \\ M_M &= \frac{PK_{WD}(K_{WD} + K_M)^2}{2\pi G \sin^3 i}. \end{aligned} \quad (2)$$

The actual mass of the white dwarf can be determined from the gravitational redshift and the mass-radius relationship for white dwarfs (Althaus & Benvenuto 1997). First we calculate the difference in systemic velocities for both system components ($\gamma_{WD} - \gamma_M$). We must then add corrections for (i) the redshift of the M dwarf, GM_M/R_{Mc} , where the radius of the M dwarf has been calculated by using the mass-radius relationship given by Caillault & Patterson (1990):

$$\log R/R_\odot = 0.796 \log M/M_\odot - 0.037,$$

(ii) the difference in transverse Doppler shifts of both components:

$$(K_M^2 - K_{WD}^2)/2c \sin^2 i,$$

(iii) the potential at the M dwarf produced by the white dwarf:

$$GM_{WD}/ac,$$

(iv) and the potential at the white dwarf due to the M dwarf:

$$GM_M/ac,$$

where a is the distance between both stars. The mass of the white dwarf is then calculated by comparing the resulting gravitational redshift with models for low mass helium white dwarfs (Althaus & Benvenuto 1997; Benvenuto & Althaus 1998). The inclination of the system can then be calculated by using Eq. 2.

In order to calculate the corrections to the white dwarf's

Table 8. Summary of the parameters for WD1042–690 and WD2009+622. BA indicates Benvenuto & Althaus (1998). See text for explanations on the different values given.

Parameter	white dwarf	M dwarf
WD1042–690		
$f_m(M_\odot)$	0.0116(2)	0.00013(1)
$M(M_\odot)$ from Eq 2	0.0174(9)	0.0039(4)
$M(M_\odot)$ from q	0.75(5)/0.78(5)	0.1665(5)/0.1735(5)
$M(M_\odot)$ from BA	0.75(7)/0.78(7)	
$M(M_\odot)$ if CO WD	0.72	
i ($^\circ$)	16	
WD2009+622		
$f_m(M_\odot)$	0.233(4)	0.0065(5)
$M(M_\odot)$ from Eq 2	0.40(3)	0.12(2)
$M(M_\odot)$ from q	0.61(3)/0.64(3)	0.1845(5)/0.1925(5)
$M(M_\odot)$ from BA	0.61(3)/0.64(3)	
$M(M_\odot)$ if CO WD	0.59	
i ($^\circ$)	60/59	

gravitational redshift we had to assume a value for the mass of the M dwarf. We performed several iterations of these calculations until we obtained consistent values for all the parameters. This method has been used previously (Marsh & Duck 1996; Maxted et al. 1998) to obtain the masses of both components in pre-CV systems. The results obtained after these iterations are presented in Table 8.

We chose as the best estimates for the corrections described above and the final parameters of the iterations, those that resulted in a mass for the white dwarf that was closer to that calculated by Benvenuto & Althaus (1998). A minimum value for the masses of the components was found when we assumed a helium core white dwarf, with metallicity $Z = 0.001$ and an outer hydrogen envelope of fractional mass (i.e. mass of envelope/total mass of the star) 10^{-8} . We assumed a $T_{\text{eff}} = 21380$ K and 25870 K for WD1042–690 and WD2009+622 respectively (Bragaglia, Renzini & Bergeron 1995; Bergeron, Saffer & Liebert. 1992). A maximum value was found if instead we assumed that the fractional mass of the outer hydrogen envelope was 4×10^{-4} in the case of WD1042–690 and 2×10^{-4} in the case of WD2009+622. The minimum and maximum values found for the masses are given in Table 8.

For WD1042–690, $\gamma_{WD} - \gamma_M$ is 36.16 ± 2.72 km s $^{-1}$. After iterating for different values for the mass of the M dwarf we find that if M_M is 0.166 - 0.167 M_\odot the corrections i, ii, iii and iv are respectively 0.48, 0.09, 0.24 and -0.05 km s $^{-1}$, giving a value for the white dwarf redshift of 36.92 km s $^{-1}$. If, on the other hand, M_M is 0.173 - 0.174 M_\odot the corrections are respectively 0.48, 0.10, 0.25, -0.05 km s $^{-1}$, giving a value for the white dwarf redshift of 36.93 km s $^{-1}$.

For WD2009+622, $\gamma_{WD} - \gamma_M$ is 26.20 ± 0.78 km s $^{-1}$. For a mass for the $M_M = 0.184 - 0.185$ M_\odot or between 0.192 - 0.193 M_\odot , the values for i, ii, iii, and iv are 0.49, 0.04, 0.12 and -0.04 km s $^{-1}$, giving 26.82 km s $^{-1}$ for the white dwarf redshift.

If a carbon-oxygen core white dwarf with metallicity $Z=0$ and a hydrogen envelope of fractional mass 10^{-4} is assumed instead, the values obtained for the masses of the white dwarf are 0.72 and 0.59 M_\odot for WD1042–690 and WD2009+622 respectively.

Table 9. New values for the M dwarf parameters depending on its filling factor f for WD2009+622. R_{MCP} is the radius calculated from the equation of Caillault & Patterson (1990) given in Section 3.3.2. A range of values for several parameters are given. These are the result of assuming two different masses for the outer hydrogen envelope of the white dwarf. See text for details.

f	K_{M} km s^{-1}	q	M_{M} M_{\odot}	i $^{\circ}$	a R_{\odot}	R_{M} R_{\odot}	R_{MCP} R_{\odot}
0.0	144.72	0.30	0.184 – 0.192	60 – 59	3.191 – 3.234	0.0	0.239 – 0.247
0.1	149.95	0.29	0.178 – 0.185	63 – 62	3.182 – 3.225	0.085 – 0.087	0.233 – 0.240
0.2	155.58	0.28	0.172 – 0.179	67 – 65	3.173 – 3.216	0.171 – 0.173	0.226 – 0.233
0.3	161.64	0.27	0.165 – 0.172	72 – 70	3.165 – 3.207	0.256 – 0.260	0.219 – 0.226
0.4	168.20	0.26	0.159 – 0.165	80 – 76	3.156 – 3.198	0.342 – 0.346	0.212 – 0.219
0.5	175.30	0.25	0.152 – 0.159	79 – 84	3.147 – 3.190	0.427 – 0.433	0.205 – 0.212
0.6	183.04	0.24	0.146 – 0.152	72 – 74	3.138 – 3.180	0.513 – 0.520	0.199 – 0.205
0.7	191.49	0.23	0.140 – 0.145	67 – 69	3.129 – 3.171	0.598 – 0.606	0.192 – 0.198
0.8	200.76	0.22	0.133 – 0.139	64 – 65	3.120 – 3.162	0.684 – 0.693	0.184 – 0.190
0.9	210.97	0.21	0.127 – 0.132	61 – 62	3.111 – 3.153	0.769 – 0.780	0.177 – 0.183
1.0	222.28	0.20	0.120 – 0.125	59 – 59	3.102 – 3.144	0.855 – 0.866	0.170 – 0.176

The masses obtained for both white dwarfs are unusually high indicating that the star probably reached the asymptotic giant branch (AGB) in its evolution. The initial binaries must have been very wide in order for this to happen. We notice that the masses calculated here differ significantly from those given in Section. 4, measured by fitting the line profiles to stellar atmosphere models. This discrepancy suggests that the redshift measurements may not be reliable, perhaps not surprising given the difficulty of separating the M star emission from the white dwarf absorption. Measurements of the white dwarf at UV wavelengths would be helpful.

As mentioned in Section 3.3.1, the flux modulation seen in Fig. 7 for WD2009+622 indicates that the M dwarf companion is strongly irradiated and therefore the value measured for K_{M} is probably a lower limit for the true radial velocity semiamplitude. This implies that the M dwarf mass and inclination given in Table 8 are upper and lower limits respectively. To calculate how distorted the M dwarf is, we calculate how much the radial velocity semiamplitude of the companion changes as a function of its radius and how its mass and inclination are affected. We present the results in Table 9. The radius of the M dwarf is given in terms of a linear filling fraction, f , defined as the ratio of the stellar radius measured from the centre of mass to the inner Lagrangian point. A value of $f = 1$ implies that the M dwarf fills its Roche lobe. For these calculations we have taken $M_{\text{WD}} = 0.61$ and $0.64 M_{\odot}$ (the maximum and minimum values calculated above) and $K_{\text{WD}} = -43.81 \text{ km s}^{-1}$. If the M star does not deviate too far from the main sequence we expect it to fill at least 0.4 of its Roche lobe which translates into a true radial velocity semiamplitude in the range $168 < K_{\text{M}} < 222 \text{ km s}^{-1}$, and a mass between $0.120 < M_{\text{M}} < 0.165 M_{\odot}$.

3.3.3 The masses of the M dwarf companions

An independent estimate of the masses of the M type companions can be done from their absolute infrared magnitudes. Although the white dwarfs dominate the flux in the optical range in both systems, they produce only a minor fraction of the infrared luminosity. The distances of the systems were computed from the parameters of the white dwarfs given in Section 4. Since the flux contribution of the M dwarfs in the blue part of the spectra, used for the model

atmosphere fits, is very small, we do not expect systematic effects caused by spectral contamination.

J, H, and K magnitudes were retrieved from the 2MASS point source catalogue. We computed the white dwarf's contribution using the colour calibration of Bergeron et al. (1995) and subtracted it from the observed fluxes. Corrections are small for WD1042–690 and do not exceed 25% (10%) for the J (K) band flux of WD2009+622. Finally, the M dwarf masses were computed from the calibration of Henry & McCarthy (1993). Results are listed in Table 10. Our error estimates include photometric errors and distance uncertainties resulting from the spectral analysis of the white dwarf. We adopted Napiwotzki, Green & Saffer's (1999) estimates for the external fit errors.

For both systems, the value obtained for the mass of the M dwarf companion from its infrared magnitudes is in agreement with that obtained from the spectral analysis in section 3.3.2. In the case of WD2009+622, the revised mass after taking into account heating by the white dwarf is considered.

4 DISCUSSION

Table 11 gives a list of all the detached white-dwarf binaries with known orbits known up to now. Most values have been taken from Ritter & Kolb (2003). The 6 systems discussed in this paper are also included.

Liebert, Bergeron & Holberg (2005), Bergeron et al. (1992) and Bragaglia et al. (1995) obtain the temperatures and gravities for the systems studied in this paper. Their values, together with our determination for the masses of the white dwarf, are given in Table. 12.

Fig. 9 presents the theoretical mass versus orbital period distribution for DDs from the population model as described in Nelemans et al. (2004). The four DDs discussed in this paper are plotted over the theoretical distribution and fall right in the expected range of values according to Nelemans et al. (2004).

The direct progenitors of the double white dwarf binaries (giant plus white dwarf) could have had a wide variety of masses and periods, leading to inferred efficiencies of the CE that are poorly constrained (see Nelemans & Tout 2004, fig. 5).

We calculated the possible progenitor systems of the

Table 10. Infrared properties and mass estimates for the M dwarf companions.

	dist (pc)	M_J	M_H	M_K	M/M_\odot
WD1042–690	34.8 ± 2.5	8.71 ± 0.16	8.18 ± 0.16	7.85 ± 0.16	0.169 ± 0.010
WD2009+622	115 ± 9	9.28 ± 0.18	8.80 ± 0.18	8.39 ± 0.18	0.136 ± 0.009

Table 11. List of all the detached white dwarf binaries with known orbital periods (given in days). The type of binary is also given where WD = white dwarf; M = M dwarf; sdO/sdB = O/B subdwarf; ? = uncertain. * indicates periods measured in this paper. References for the orbital periods not measured in this paper are (a) Bragaglia, Greggio & Renzini 1990, (b) Koen, Orosz & Wade 1998, (c) Orosz & Wade 1999, (d) Maxted et al. 2000a, (e) Morales-Rueda et al. 2003a, (f) Maxted et al. 2000b, (g) Marsh 1995, (h) Marsh et al. 1995, (i) Moran et al. 1999, (j) Saffer, Livio & Yungelson 1998, (k) Napiwotzki et al. 2002, (m) Maxted, Marsh & Moran 2002, (n) Holberg et al. 1995, (o) Drechsel et al. 2001, (p) Kilkenny et al. 1998, (q) Maxted et al. 1998, (r) Wood & Saffer 1999, (s) Orosz et al. 1999 (t) Bruch & Diaz 1998, (u) Gizis 1998, (v) Wood, Harmer & Lockley 1999 (w) Delfosse et al. 1999 (x) Napiwotzki et al. 2001, (y) Maxted et al. 2000c, (z) Saffer, Liebert & Olszewski 1988, (aa) Heber et al. 2003, (ab) Karl et al. 2003, (ac) O’Donoghue et al. 2003, (ad) Maxted et al. 2002, (ae) Hillwig et al. 2002, (af) Maxted et al. 2004, (ag) Kawka et al. 2000, (ah) Kawka et al. 2002, (ai) Saffer et al. 1993, (aj) O’Brien, Bond & Sion 2001, (ak) Sing et al. 2004, (al) Moran, Marsh & Bragaglia 1997, (am) Morales-Rueda et al. 2003b, (an) Edelmann, Heber & Napiwotzki 2002, (ao) Napiwotzki et al. 2004, (ap) Fuhrmeister & Schmitt 2003, (aq) O’Toole, Heber & Benjamin 2004, (ar) Robb & Greimel 1997, (as) Heber et al. 2004, (at) Raymond et al. 2003, (au) Gänsicke et al. 2004, (av) Wood, Robinson & Zhang 1995, (aw) Bruch, Vaz & Diaz 2001, (ax) Pigulski & Michalska 2002, (ay) Shimansky, Borisov & Shimanskaya 2003, (az) Rauch & Werner 2003, (ba) Chen et al. 1995, (bb) Green, Richstone & Schmidt 1978, (bc) Landolt & Drilling 1986, (bd) Bell, Pollacco & Hilditch 1994, (be) Pollacco & Bell 1994, (bf) Lanning & Pesch 1981, (bg) Bleach et al. 2002, (bh) Vennes & Thorstensen 1994.

WD, sdOB + WD Object	P_{orb}	Type	Ref.	WD, sdOB + M Object	P_{orb}	Type	Ref.	sdOB + ? Object	P_{orb}	Ref.
WD0957–666	0.061	WD/WD	a, al	PG1017–086	0.073	sdB/M	m	HE0532–4503	0.266	ao
KPD0422+5421	0.090	sdB/WD	b, c	HS0705+6700	0.096	WD/M	o	PG1528+104	0.331	am
KPD1930+2752	0.095	sdB/WD	d	PG1336–018	0.101	sdB/M	p	KPD1946+4340	0.404	e
PG1043+760	0.120	sdB/WD	e	GD448	0.103	WD/M	q	HE0929–0424	0.440	ao
PG1101+364	0.145	WD/WD	g	MT Ser	0.113	sdO/M	aw	HE1318–2111	0.487	ao
WD1704+481	0.145	WD/WD	f	HW Vir	0.117	sdB/M	r	PG1743+477	0.515	e
WD2331+290	0.166	WD/WD	h	HS2237+8154	0.124	WD/M	au	PG0001+275	0.528	an
PG1432+159	0.225	sdB/WD	i	NN Ser	0.130	WD/M	ax	PG1519+640	0.539	am
PG2345+318	0.241	sdB/WD	i	EC13471–1258	0.151	WD/M	ac	HE1059–2735	0.556	ao
HE2209–1444	0.277	WD/WD	ab	J1129+6637	0.171	WD/M	at	PG1725+252	0.601	e
PG1101+249	0.354	sdB/WD	j, i	HS2333+3927	0.172	sdB/M	as	PG1247+554	0.603	d
Feige 48	0.376	sdB/WD	aq	GD245	0.174	WD/M	ay	HD188112	0.607	aa
HE1414–0848	0.518	WD/WD	k	BPM71214	0.202	WD/M	ah	PG1627+017	0.829	e
PG0101+039	0.570	sdB/WD	i	PG1329+159	0.250	sdB/M	e	PG1230+052	0.837	am
PG1248+164	0.732	sdB/WD	e	PG1224+309	0.259	WD/M	s	HE2135–3749	0.924	ao
PG0849+319	0.745	sdB/WD	e	AA Dor	0.261	sdO/M	az	PG0133+144	1.238	e, an
PG1116+301	0.856	sdB/WD	e	WD2154+408	0.268	WD/M	ae	PG1512+244	1.270	e
PG0918+029	0.877	sdB/WD	e	CC Cet	0.287	WD/M	ai	UVO1735+22	1.278	an
WD1713+332	1.123	WD/WD	h	RR Cae	0.304	WD/M	t	HE2150–0238	1.322	ao
WD1428+373	1.143	WD/WD	*	TW Crv	0.328	sdO/M	ba	KPD2040+3955	1.483	am
WD1022+050	1.157	WD/WD	*	WD1042–690	0.336	WD/M	*, ag	HD171858	1.529	e
HE1047–0436	1.213	sdB/WD	x	GK Vir	0.344	WD/M	bb	PG1716+426	1.777	e
WD0136+768	1.407	WD/WD	m	KV Vel	0.357	WD/M	bc	PG1300+279	2.259	e
Feige55	1.493	WD/WD	n	RXJ1326+4532	0.364	WD/M	ar	KPD0025+5402	3.571	e
L870-2	1.556	WD/WD	z	UU Sge	0.465	WD/M	bd	PG0934+186	4.05	am
WD1204+450	1.603	WD/WD	m	V447 Lyr	0.472	sdO/M	be	PG0839+399	5.622	e
PG1538+269	2.50	sdB/WD	j	V1513 Cyg	0.497	WD/M	u	PG1244+113	5.752	am
WD1241–010	3.347	WD/WD	h	V471 Tau	0.521	WD/K	aj	HE115–0631	5.87	ao
WD1317+453	4.872	WD/WD	h	RXJ2130+4710	0.521	WD/M	af	PG0907+123	6.116	e
WD2032+188	5.084	WD/WD	*	HZ 9	0.564	WD/M	bf	PG1032+406	6.779	e
WD1824+040	6.266	WD/WD	*	PG1026+002	0.597	WD/M	v	WD0048–202	7.45	ao
PG1115+166	30.09	WD/WD	ad	EG UMa	0.668	WD/M	bg	WD0940+068	8.33	d
				REJ2013+400	0.706	WD/M	v	PG1110+294	9.415	e
				WD2009+622	0.741	WD/M	*	PG1619+522	15.357	e
				REJ1016–0520	0.789	WD/M	v	PG0850+170	27.81	e
				HS1136+6646	0.836	WD/K	ak			
				IN CMa	1.263	WD/M	ah			
				BE UMa	2.291	WD/K	av			
				REJ1629+780	2.89	WD/M	ap			
				Feige 24	4.232	WD/M	bh			
				G203–047ab	14.71	WD/M	w			

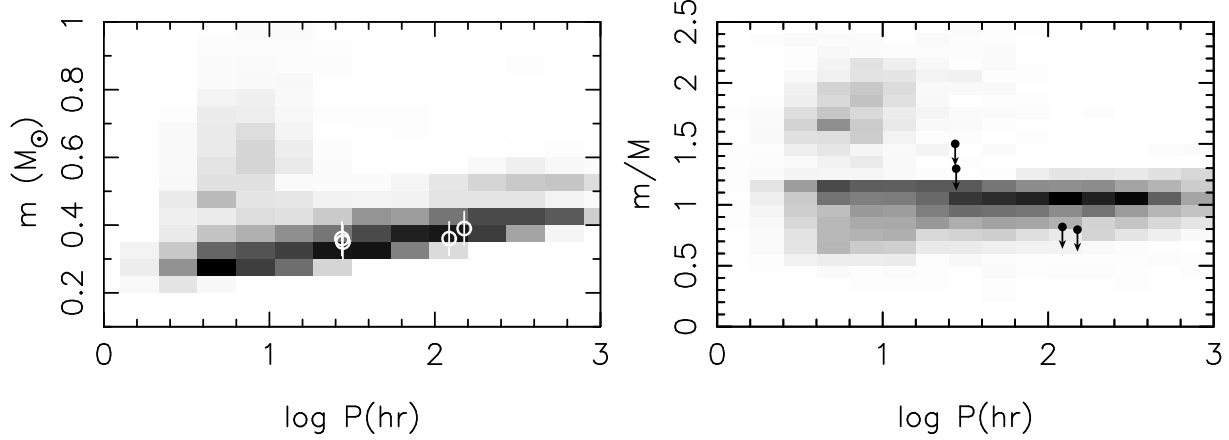


Figure 9. Left panel: mass of the bright white dwarf for the four DDs discussed in this paper as measured by Bragaglia et al. (1995), Liebert et al. (2005) and Bergeron et al. (1992) (see Table 5) versus period distribution. In the grey scale we plot the mass to period distribution of DDs according to theory (for the model described in Nelemans et al. (2004)). Right panel: mass ratio (only upper limits taken from Table 5) for the four DDs studied versus period distribution. The theoretical distribution according to the Nelemans et al. (2004) is also plotted.

Table 12. Temperatures and gravities measured for the bright component of the system by fitting the hydrogen line profiles to stellar atmosphere models. (a) Bragaglia et al. (1995), (b) Liebert et al. (2005) and (c) Bergeron et al. (1992). V represents the V magnitude taken from the literature and M_V is the absolute magnitude. The masses given have been determined using cooling tracks by Althaus & Benvenuto (1997).

WD	V	$T_{\text{eff}}(K)$	$\log g$	M/M_{\odot}	M_V	Ref
1022+050	14.18	14481	7.48	0.389	10.68	a
1428+373	15.40	14010	7.36	0.348	10.35	b
1824+040	13.90	14795	7.61	0.428	10.83	a
2032+188	15.34	18540	7.48	0.406	10.24	c
1042-690	13.09	21380	7.86	0.551	10.52	a
2009+622	15.15	25870	7.70	0.489	9.93	c

two white dwarf plus M star binaries. If the high masses inferred from the gravitational redshifts were right, this means the direct progenitors of the white dwarfs must have been highly evolved giants. Using the equations in Hurley, Pols & Tout (2000) in the same way as described in Nelemans & Tout (2004) we calculated the possible progenitor systems. For WD1042-690 we find possible progenitors with masses typically in the range $2 - 3.5 M_{\odot}$, while for WD2009+622 the progenitors typically have masses between $1.25 - 3 M_{\odot}$. Because of the rather extreme mass ratios and the large radii of the giants, the CE is most likely caused by tidal interaction, rather than Roche-lobe overflow (Hut 1980) and the binaries will generally not be synchronised. We use the formalism derived for star - planet interactions by Soker (1996) to calculate the separation between the two stars at which the CE sets in. The required CE efficiencies are between 0.1 and 1 for WD1042-690 and between 0.1 and 1.6 for WD2009+622. Both systems can also be explained with the gamma-algorithm (Nelemans & Tout 2004), with values of γ around 1.5. If, on the other hand, the lower white dwarf masses presented in Table 12 are right, the progenitor masses inferred are in the range $0.9 - 2.5 M_{\odot}$ for WD1042-690 and

$0.75 - 2 M_{\odot}$ for WD2009+622. The required CE efficiencies derived in this case lie in the same ranges as for the more massive white dwarf alternative presented above.

Using the binary results presented in Tables 7 and 8, and the equations from Schreiber & Gänsicke (2003), we have calculated the white dwarf cooling age using models by Wood, Robinson & Zhang (1995), t_{cool} , the orbital period of the binary at the end of the CE phase, P_{CE} , the time it will take for the binary to start mass transfer (and become a CV) assuming classical magnetic braking (CMB) and assuming reduced magnetic braking (RMB), t_{sd} , and the orbital period when mass transfer starts, P_{sd} . These values are presented in the top three rows of Table 13. The input masses used for the white dwarfs are those obtained assuming that they are carbon-oxygen core white dwarfs. The input masses for the companions are $0.17 M_{\odot}$ for WD1042-690 and $0.120 < M_M < 0.165 M_{\odot}$ for WD2009+622 (as calculated in Section 3.3.2). The value of P_{CE} for both binaries is very close to their present orbital periods which indicates that they are very young PCEBs. These systems will not become CVs within a Hubble time (except perhaps WD1042-690 if RMB takes place), assuming $\tau_0 = 1.3 \times 10^{10}$ yrs (Ferrerias, Melchiorri & Silk 2001), and when they do, their orbital periods will place them below the CV period gap.

The evolutionary properties of WD1042-690 and WD2009+622 are also calculated by using the lower white dwarf masses presented in Table 12 and the masses of the M dwarfs obtained in Section 3.3.3. These are presented in the bottom two rows of Table 13. The values for all parameters in this case are similar to those obtained for the larger white dwarf masses and the conclusions reached are equivalent.

5 CONCLUSIONS

We have obtained the orbital solution for four DD systems and two white dwarf - M dwarf binaries. We find that the white dwarf companions for the four DDs studied contribute between 10 and 20 per cent of the total luminosity and

Table 13. Evolutionary properties of WD1042–690 and WD2009+622. The top three rows present the results obtained assuming the white dwarf masses given in Table 8 (0.72 and 0.59 M_{\odot} respectively). ¹ and ² indicate calculations obtained for WD2009+622 by assuming $M_M = 0.12$ and 0.165 M_{\odot} respectively. The bottom two rows present the results obtained when the lower white dwarf masses given in Table 12 are assumed instead. In this case the M dwarf masses calculated in Section 3.3.3 are used. The values of t_{cool} and t_{sd} given in the table are in fact the logs of t_{cool} and t_{sd} in years.

WD	t_{cool}	P _{CE} (d)		t_{sd}		P _{sd} (d)
		CMB	RMB	CMB	RMB	
1042–690	7.92	0.3381	0.3375	10.30	10.08	0.073
2009+622 ¹	7.31	0.7412	0.7411	11.43	10.96	0.055
2009+622 ²	7.31	0.7412	0.7411	11.30	10.78	0.071
1042–690	7.65	0.3376	0.3372	10.39	10.09	0.073
2009+622	7.20	0.7412	0.7410	11.43	10.87	0.061

remain undetected. The masses and periods obtained for these systems agree with theoretical mass period distributions (based on Nelemans et al. (2004)).

In the case of the white dwarf - M dwarf binaries we have been able to measure the motion of both components. We find that there are signatures of strong irradiation of the surface of the M dwarf component in WD2009+622. The white dwarf masses calculated from their gravitational redshift are unusually high compared to those measured by fitting their hydrogen lines with stellar atmosphere models, and could be the result of the evolution of giant stars with masses between 1.25 and 3.5 M_{\odot} that went through a CE phase as a result of tidal interaction. These two binaries are young PCEBs that will evolve into CVs, although not within a Hubble time, with orbital periods below the period gap.

ACKNOWLEDGEMENTS

LMR was supported by a PPARC post-doctoral grant and by NWO-VIDI grant 639.042.201 to P.J. Groot during the course of this research. GN is supported by PPARC and an NWO-VENI grant. TRM acknowledges the support of a PPARC Senior Research Fellowship. RN acknowledges support by a PPARC Advanced Fellowship. The authors would like to thank M. R. Schreiber for his help with implementing the calculations for this paper. The reduction and analysis of the data were carried out on the Southampton node of the STARLINK network. We thank PATT for their support of this program.

REFERENCES

Althaus L. G., Benvenuto O. G., 1997, ApJ, 477, 313
 Bell S. A., Pollacco D. L., Hilditch R. W., 1994, MNRAS, 270, 449
 Benvenuto O. G., Althaus L. G., 1998, MNRAS, 293, 177
 Bergeron P., Saffer R. A., Liebert J., 1992, ApJ, 394, 228
 Bergeron P., Wesemael F., Beauchamp A., 1995, PASP, 107, 1047
 Bleach J. N., Wood J. H., Smalley B., Catalan M. S., 2002, MNRAS, 336, 611
 Bragaglia A., Greggio L., Renzini A., 1990, ApJ, 365, L13
 Bragaglia A., Renzini A., Bergeron P., 1995, ApJ, 443, 735

Bruch A., Diaz M. P., 1998, AJ, 116, 908
 Bruch A., Vaz L. P. R., Diaz M. P., 2001, A&A, 377, 898
 Caillault A.-P., Patterson J., 1990, AJ, 100, 825
 Chen A., O’Donoghue D., Stobie R. S., Kilkenny D., Roberts G., van Wyk F., 1995, MNRAS, 275, 100
 Cumming A., Marcy G. W., Butler R. P., 1999, ApJ, 526, 890
 Delfosse X., Forveille T., Beuzit J.-L., Udry S., Mayor M., Perrier C., 1999, A&A, 344, 897
 Drechsel H. et al., 2001, A&A, 379, 893
 Edelmann H., Heber U., Napiwotzki R., 2002, AN, 322, 401
 Ferreras I., Melchiorri A., Silk J., 2001, MNRAS, 327, L47
 Fuhrmeister B., Schmitt J. H. M. M., 2003, A&A, 403, 247
 Gänsicke B. T., Araujo-Betancor S., Hagen H.-J., Harlaftis E. T., Kitsionas S., Dreizler S., Engels D., 2004, A&A, 418, 265
 Gizis J. E., 1998, AJ, 115, 2053
 Green R. F., Richstone D. O., Schmidt M., 1978, ApJ, 224, 892
 Heber U., Edelmann H., Lisker T., Napiwotzki R., 2003, A&A, 411, 1477
 Heber U. et al., 2004, A&A, 420, 251
 Henry T. J., McCarthy D. W. Jr., 1993, AJ, 106, 773
 Hillwig T. C., Gale A. A., Honeycutt R. K., Rengstorf A. W., 2002, PASP, 114, 756
 Holberg J. B., Saffer R. A., Tweedy R. W., Barstow M. A., 1995, ApJ, 452, 133
 Hurley J. R., Pols O. R., Tout C. A., 2000, MNRAS, 315, 543
 Hut P., 1980, A&A, 92, 167
 Iben I., Tutukov A. V., 1984, ApJS, 54, 335
 Karl C. A., Napiwotzki R., Nelemans G., Chrislieb N., Koester D., Heber U., Reimers D., 2003, A&A, 410, 663
 Kawka A., Vennes S., Dupuis J., Koch R., 2000, AJ, 120, 3250
 Kawka A., Vennes S., Koch R., Williams A., 2002, AJ, 124, 2853
 Kilkenny D., O’Donoghue D., Koen C., Lynas-Gray A. E., van Wyk F., 1998, MNRAS, 296, 329
 Koen C., Orosz J. A., Wade R. A., 1998, MNRAS, 300, 659
 Landolt A. Drilling J. S., 1986, AJ, 91, 1372
 Lanning H. H., Pesch P., 1981, ApJ, 244, 280
 Liebert J., Bergeron P., Holberg J. B., 2005, ApJS, 156, 47L
 Lomb N. R., 1976, Ap&SS, 39, 447
 Marsh T. R., 1989, PASP, 101, 1032
 Marsh T. R., 1995, MNRAS, 275, 1
 Marsh T. R., Duck S. R., 1996, MNRAS, 278, 565
 Marsh T. R., Horne K., 1988, MNRAS, 235, 269
 Marsh T. R., Dhillon V. S., Duck S. R., 1995, MNRAS, 275, 828
 Maxted P. F. L., Marsh T. R., Moran C. K. J., Dhillon V. S., Hilditch R. W., 1998, MNRAS, 300, 1225
 Maxted P. F. L., Moran C. K. J., Marsh T. R., Gatti A. A., 2000a, MNRAS, 311, 877
 Maxted P. F. L., Marsh T. R., Moran C. K. J., Han Z., 2000b, MNRAS, 314, 334
 Maxted P. F. L., Marsh T. R., Moran C. K. J., 2000c, MNRAS, 319, 305
 Maxted P. F. L., Burleigh M. R., Marsh T. R., Bannister N. P., 2002, MNRAS, 334, 833
 Maxted P. F. L., Marsh T. R., Moran C. K. J., 2002, MNRAS, 332, 745
 Maxted P. F. L., Marsh T. R., Morales-Rueda L., Barstow M. A., Dobbie P. D., Schreiber M. R., Dhillon V. S., Brinkworth C. S., 2004, MNRAS, 355, 178
 Morales-Rueda L., Maxted P. F. L., Marsh T. R., North R. C., Heber U., 2003a, MNRAS, 338, 752
 Morales-Rueda L., Marsh T. R., North R. C., Maxted P. F. L., 2003b, Proceedings of the Thirteen European Workshop on White Dwarfs. NATO Science Series, 105, 57
 Moran C., Marsh T. R., Bragaglia A., 1997, MNRAS, 288, 538
 Moran C., Maxted P., Marsh T. R., Saffer R. A., Livio M., 1999, MNRAS, 304, 535
 Napiwotzki R., Green P. J., Saffer R. A., 1999, AJ, 517, 399

- Napiwotzki R., Edelmann H., Heber U., Karl C., Drechsel H., Pauli E.-M., Christlieb N., 2001, *A&A*, 378, 17
- Napiwotzki R. et al., 2002, *A&A*, 386, 957
- Napiwotzki R. et al., 2003, *Proceedings of the Thirteen European Workshop on White Dwarfs. NATO Science Series*, 105, 39
- Napiwotzki R., Karl C. A., Lisker T., Heber U., Christlieb N., Reimers D., Nelemans G., Homeier D., 2004, *Ap&SS*, 291, 321
- Napiwotzki R. et al., 2005, *A&A*, submitted
- Nelemans G., Tout C. A., 2004, *MNRAS*, 356, 753
- Nelemans G., Yungelson L. R., Portegies Zwart S. P., Verbunt F., 2001, *A&A*, 365, 491
- Nelemans G., Yungelson L. R., Portegies Zwart S. P., 2004, *MNRAS*, 349, 181
- O'Brien M. S., Bond H. E., Sion E. M., 2001, *ApJ*, 563, 971
- O'Donoghue D., Koen C., Kilkeny D., Stobie R. S., Koester D., Bessel M. S., Hambly N., MacGillivray H., 2003, *MNRAS*, 345, 506
- Orosz J. A., Wade R. A., 1999, *MNRAS*, 310, 773
- Orosz J. A., Wade R. A., Harlow J. J. B., Thorstensen J. R., Taylor C. J., Eracleous M., 1999, *AJ*, 117, 1598
- O'Toole S. J., Heber U., Benjamin R. A., 2004, *A&A*, 422, 1053
- Piersanti L., Gagliardi S., Iben I. Jr, Tornambé A., 2003, *ApJ*, 583, 885
- Pigulski A., Michalska G., 2002, *IBVS* 5218
- Pollacco D. L., Bell S. A., 1994, *MNRAS*, 267, 452
- Rauch T., Werner K., 2003, *A&A*, 400, 271
- Raymond S. N. et al., 2003, *AJ*, 125, 2621
- Ritter H., Kolb U., 2003, *A&A*, 404, 301
- Robb R. M., Greimel R., 1997, *IBVS* 4486
- Saffer R., Wade R. A., Liebert J., Green R. F., Sion E. M., Bechtold J., Foss D., Kidder K., 1993, *AJ*, 105, 1945
- Saffer R. A., Liebert J., Olszewski E. W., 1988, *ApJ*, 334, 947
- Saffer R. A., Livio M., Yungelson L. R., 1998, *ApJ*, 502, 394
- Saio H., Nomoto K., 1998, *ApJ*, 500, 388
- Scargle J. D., 1982, *ApJ*, 263, 835
- Schreiber M. R., Gänsicke B. T., 2003, *A&A*, 406, 305
- Shimansky V. V., Borisov N. V., Shimanskaya N. N., 2003, *Astron. Rep.* 47, 763
- Silvestri N. M., Hawley S. L., Szkody P., 2003, *AAS*, 203, 4201
- Sing D. K. et al., 2004, *AJ*, 127, 2936
- Soker N., 1996, *ApJ*, 460, L53
- Soker N., Harpaz A., 2003, *MNRAS*, 343, 456
- Vennes S., Thorstensen J. R., 1994, *AJ*, 108, 1881
- Wood J. H., Saffer R., 1999, *MNRAS*, 305, 820
- Wood J. H., Robinson E. L., Zhang E.-H., 1995, *MNRAS*, 277, 87
- Wood J. H., Harmer S., Lockley J. J., 1999, *MNRAS*, 304, 335